LETTER

doi:10.1038/nature11466

# Dopaminergic neurons inhibit striatal output through non-canonical release of GABA

Nicolas X. Tritsch[1], Jun B. Ding[1]† & Bernardo L. Sabatini[1]

**The substantia nigra pars compacta and ventral tegmental area contain the two largest populations of dopamine-releasing neurons in the mammalian brain. These neurons extend elaborate projections in the striatum, a large subcortical structure implicated in motor planning and reward-based learning. Phasic activation of dopaminergic neurons in response to salient or reward-predicting stimuli is thought to modulate striatal output through the release of dopamine to promote and reinforce motor action[1–4]. Here we show that activation of dopamine neurons in striatal slices rapidly inhibits action potential firing in both direct- and indirect-pathway striatal projection neurons through vesicular release of the inhibitory transmitter GABA (γ-aminobutyric acid). GABA is released directly from dopaminergic axons but in a manner that is independent of the vesicular GABA transporter VGAT. Instead, GABA release requires activity of the vesicular monoamine transporter VMAT2, which is the vesicular transporter for dopamine. Furthermore, VMAT2 expression in GABAergic neurons lacking VGAT is sufficient to sustain GABA release. Thus, these findings expand the repertoire of synaptic mechanisms used by dopamine neurons to influence basal ganglia circuits, show a new substrate whose transport is dependent on VMAT2 and demonstrate that GABA can function as a bona fide co-transmitter in monoaminergic neurons.**

The striatum integrates inputs from cortex, hippocampus, thalamus, amygdala and ventral tegmental area/substantia nigra pars compacta (VTA/SNc) to instruct the selection of appropriate motor actions. Inputs from midbrain dopamine (DA) neurons play an important role in this process, as evidenced by the psychomotor deficits that arise after loss of these cells in Parkinson's disease, or by the occurrence of compulsive and addictive behaviours upon potentiation of dopaminergic signalling[5–7]. Through release of DA, these neurons promote activation of direct-pathway striatal projection neurons (dSPNs), which express $G\alpha_{s/olf}$-coupled $D_1$ receptors, and inhibit indirect-pathway SPNs (iSPNs), which express $G\alpha_{i/o}$-coupled $D_2$ receptors[3,5]. However, midbrain DA neurons also express neuropeptides[8] and a subset releases glutamate[9–12], suggesting that the net effects of activity in these cells may not be limited to the actions of DA.

To investigate how DA neurons influence neuronal activity in striatum, we expressed the light-activated cation channel channelrhodopsin-2 (ChR2)[13] in SNc neurons using Cre recombinase-dependent adeno-associated viruses (AAVs). In *Slc6a3*$^{IRES-Cre/wt}$ mice, Cre expression shows high penetrance and specificity for midbrain DA neurons[14] (Supplementary Fig. 1). We validated SNc targeting using an AAV encoding Cre-dependent enhanced green fluorescent protein (EGFP). Fluorescence was restricted to Cre-containing neurons in SNc, and most EGFP-expressing cells (97.9%, $n = 1587$ cells; three mice) were immunopositive for the catecholamine biosynthetic enzyme tyrosine hydroxylase, demonstrating specific expression in DA neurons (Fig. 1a, b and Supplementary Figs 1 and 2). Moreover, EGFP$^+$ axons densely innervated dorsal striatum (Fig. 1c), consistent with their nigrostriatal identity.

Carbon-fibre amperometry confirmed the ability to evoke DA release from ChR2-expressing axons in slices of dorsal striatum. Brief flashes of blue light (1 ms) reliably evoked DA transients, which were sensitive to the tyrosine hydroxylase antagonist α-methyl-tyrosine and

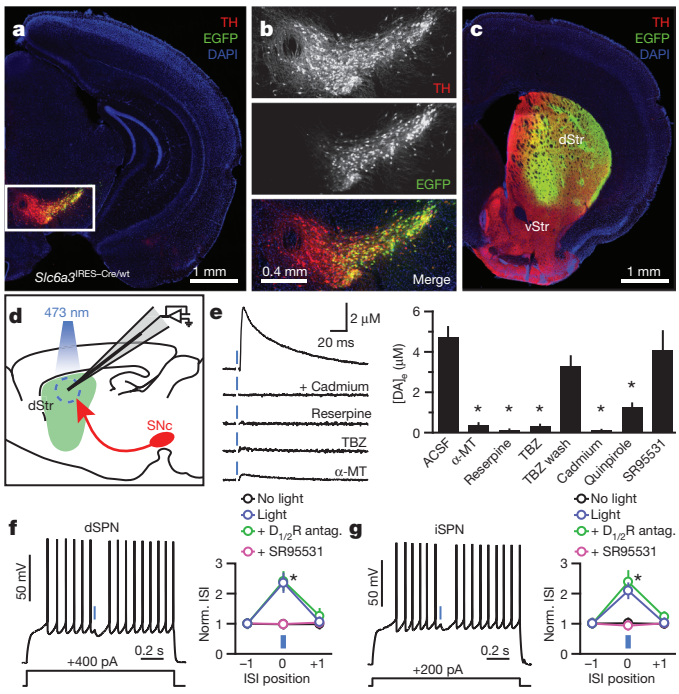


**Figure 1 | DA neuron stimulation inhibits SPNs.** **a**, Coronal midbrain section from a *Slc6a3*$^{IRES-Cre/wt}$ mouse transduced with a Cre-dependent EGFP AAV (green). DA neurons immunolabelled for tyrosine hydroxylase (TH, red). DAPI nuclear stain (blue). **b**, Higher magnification of boxed area in **a**. Although expression levels vary greatly, most EGFP$^+$ cells are tyrosine-hydroxylase-positive. **c**, EGFP$^+$ SNc neurons densely innervate dorsal striatum (dStr). vStr; ventral striatum. **d**, Carbon-fibre recording configuration in a sagittal brain slice. ChR2$^+$ DA neurons depicted red, laser illumination area blue. **e**. Left, light stimulation (blue) of DA terminals in dorsal striatum evoked cadmium-, reserpine-, TBZ- and α-methyl-tyrosine (α-MT)-sensitive DA release measured by amperometry. Stimulation artefacts blanked for clarity. Right, mean ($n = 4$–19) peak extracellular DA concentration after optogenetic stimulation of nigrostriatal axons. DA transients recovered upon TBZ washout (wash). *$P < 0.05$ versus ACSF (Mann–Whitney rank sum test). **f**, **g**, Left, membrane potential responses of a dorsal striatum dSPN (**f**) or iSPN (**g**) to current injection (1.3 s, bottom) and ChR2-mediated stimulation of DA axons (1 ms, blue). Right, average normalized duration of three consecutive interspike intervals (Norm. ISI) that precede, straddle or follow the light flash (positions '−1', '0' and '+1', respectively) upon ChR2 stimulation in ACSF (blue), DA receptor blockers ($D_{1/2}$R antagonists = SCH23390 + SKF83566 + sulpiride + L-741,626; green) or SR95531 ($GABA_A$ receptor blocker; purple). Black, light prevented from entering the sample; $n = 14$ dSPNs, 11 iSPNs. *$P < 0.05$ (two-way ANOVA). Data in **e**–**g** represent mean ± s.e.m.

[1]Department of Neurobiology, Howard Hughes Medical Institute, Harvard Medical School, 220 Longwood Avenue, Boston, Massachusetts 02115, USA. †Present address: Department of Neurology and Neurological Sciences, Stanford Institute of Neuro-innovation and Translational Neurosciences (SINTN), Stanford University School of Medicine, 1050 Arastradero Road, Palo Alto, California 94304, USA.

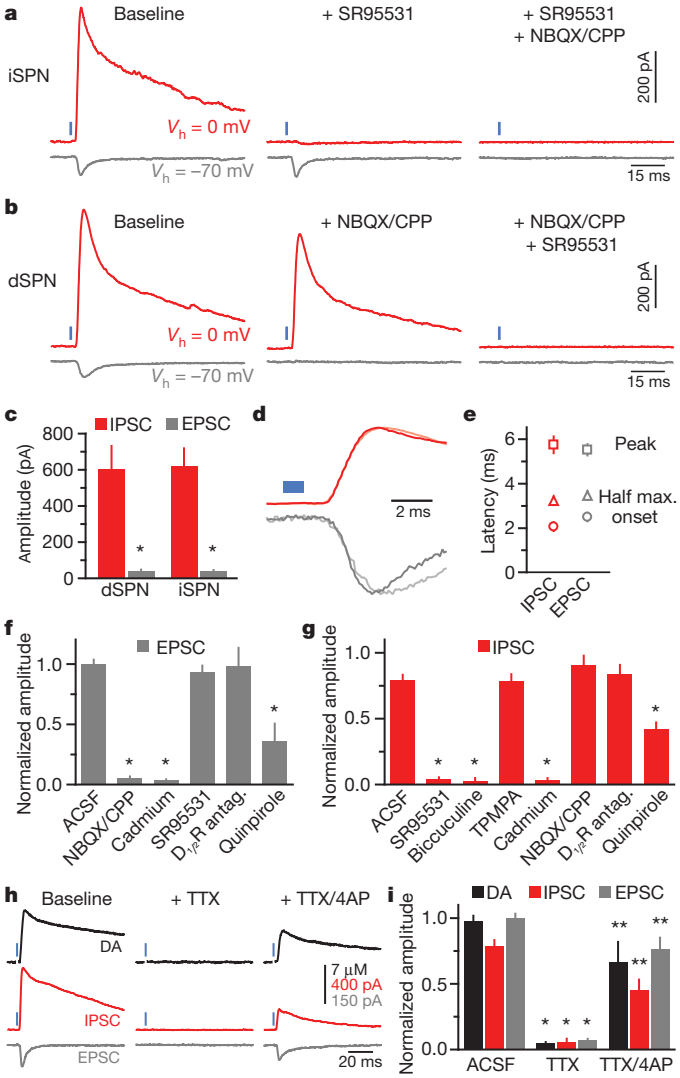


**Figure 2 | DA neurons directly release GABA onto SPNs.** **a**, Evoked current responses from an iSPN held at indicated potentials ($V_h$) to optogenetic activation of nigrostriatal axons (1 ms, blue) upon sequential bath application of SR95531 and NBQX/CPP. **b**, As in **a** for a dSPN with antagonists applied in reverse order. **c**, Mean IPSC (red) and EPSC (grey) absolute amplitudes in dSPNs ($n = 8$) and iSPNs ($n = 21$). *$P < 0.05$ versus IPSC (Mann–Whitney rank sum test). **d**, Normalized IPSCs and EPSCs from **a** (dark) and **b** (light) shown on an expanded timescale. Blue, light presentation. **e**, Average ($n = 29$ SPNs) IPSC (red) and EPSC (grey) latencies from light onset to current onset (circle), half maximal amplitude (triangle) and peak amplitude (square). IPSCs are not delayed compared with EPSCs. **f**, **g**, Mean ($n = 3$–18) EPSC (**f**) and IPSC (**g**) amplitudes under control conditions (ACSF) or in indicated antagonists normalized to baseline. *$P < 0.05$ versus ACSF (Mann–Whitney rank sum test). **h**, Amperometric DA transients (black) and current responses of a voltage-clamped iSPN ($V_h = 0$ mV, red; $V_h = -70$ mV, grey) to DA neuron stimulation under baseline conditions (left), in TTX (middle) and after co-application of TTX and 4-aminopyridine (4AP, right). **i**, Extracellular DA concentration (black), IPSC amplitude (red) and EPSC amplitude (grey) evoked by ChR2 stimulation across conditions normalized to baseline. Data from ACSF condition same as in Figs 1e and 2f, g. *$P < 0.05$ versus ACSF; ** $< 0.05$ versus TTX (Mann–Whitney rank sum test). Error bars, s.e.m.

the VMAT2 antagonists reserpine and tetrabenazine (TBZ) (Fig. 1d, e). Moreover, DA release required $Ca^{2+}$ channels, as it was blocked by cadmium, and activation of $D_2$ receptors with quinpirole reduced DA release, consistent with the effect of DA autoreceptors in nigrostriatal axons[15].

To determine the net effect of DA neuron stimulation on striatal output, we performed whole-cell current-clamp recordings from dSPNs and iSPNs in brain slices obtained from *Slc6a3*$^{IRES-Cre/wt}$;*Drd2*-EGFP mice. Whereas action potentials evoked by current steps occurred at regular intervals under baseline conditions, light presentation reliably paused firing and rapidly hyperpolarized SPNs of both populations (dSPNs: 6.8 ± 1.9 mV, $n = 10$; iSPNs: 7.0 ± 1.4 mV, $n = 7$) (Fig. 1f, g). The light-evoked pause and hyperpolarization were unaffected by a cocktail of antagonists targeting DA receptors (dSPNs: 6.6 ± 2.2 mV, $n = 4$; iSPNs: 9.5 ± 2.5 mV, $n = 4$; both $P > 0.05$ versus light only, Mann–Whitney rank sum test). Instead, they were abolished by the $GABA_A$ receptor antagonist SR95531 ($n = 4$ dSPNs, seven iSPNs) (Fig. 1f, g), which does not alter DA release (Fig. 1e). These data indicate that DA neurons exert a rapid and strong inhibitory influence on SPNs through activation of $GABA_A$ receptors.

Previous attempts at characterizing DA receptor-independent effects of DA neurons on SPNs showed a small, but rapid excitatory influence mediated by co-release of glutamate[9–12]. However, these experiments were performed in the presence of GABA receptor antagonists, precluding the detection of inhibitory influences. To observe conductances recruited after DA neuron stimulation, we performed whole-cell voltage-clamp recordings from dSPNs and iSPNs in dorsal striatum without pharmacological blockers. When SPNs were held at −70 mV ($E_{Cl}$, the reversal potential for chloride), nigrostriatal fibre stimulation evoked fast inward currents in approximately 75% of dSPNs ($n = 6/8$) and iSPNs ($n = 16/21$) (Fig. 2a–e). These currents showed similar properties in both cell types (Fig. 2a–c) and were consequently pooled for analysis: they exhibited peak amplitudes of 40 ± 5 pA ($n = 22$), rise times of 2.6 ± 0.4 ms and decay time constants of 6.8 ± 1.5 ms. Moreover, they reversed at approximately 0 mV and were sensitive to the α-amino-3-hydroxy-5-methyl-4-isoxazole propionic acid (AMPA) and NMDA (*N*-methyl-D-aspartate) receptor blockers NBQX and CPP (Fig. 2a, b, f), indicating that they are glutamatergic excitatory postsynaptic currents (EPSCs). Although glutamate release by midbrain DA neurons was proposed to be limited to mesolimbic fibres innervating ventral striatum[12], the currents reported here in dorsal striatum show similar properties[11,12], and are sensitive to the same pharmacological agents as DA release (Figs 1e and 2f), suggesting a dopaminergic origin. Moreover, EPSCs were unaffected by DA receptor antagonists (Fig. 2f), indicating that glutamate release is not secondary to DA receptor activation.

To isolate conductances that mediate SPN inhibition, the membrane potential was held at the reversal potential of ionotropic glutamate receptors (~0 mV). Under these conditions, DA neuron stimulation evoked large outward currents in all recorded dSPNs ($n = 8$) and iSPNs ($n = 21$) (Fig. 2a–c and Supplementary Fig. 3). Collectively, these currents had peak amplitudes of 617 ± 78 pA ($n = 29$; range = 0.11–1.93 nA), rise times of 2.0 ± 0.2 ms and decay time constants of 56 ± 4 ms. They reversed at $E_{Cl}$ and were blocked by SR95531 and bicuculine, but not by the $GABA_C$ receptor antagonist TPMPA (Fig. 2a, b, g), indicating that they represent $GABA_A$ receptor-mediated inhibitory postsynaptic currents (IPSCs). Similar observations were made in mice expressing Cre under control of a tyrosine hydroxylase promoter (Supplementary Fig. 4). Consistent with previous reports[11,12], no current remained with both glutamate and $GABA_A$ receptors blocked. Thus, these data show that (1) activation of dopaminergic terminals rapidly activates ionotropic glutamate and GABA receptors in SPNs, (2) the resulting currents do not differentially affect dSPNs and iSPNs, and (3) GABAergic conductances mediate the net inhibitory effect of DA neurons on striatal output.

DA neurons may activate $GABA_A$ receptors on SPNs either by recruiting a population of GABAergic interneurons—a mechanism akin to feed-forward inhibition—or by directly releasing GABA. Several lines of evidence suggest the latter. First, the latency between light and IPSC onset averaged 2.2 ± 0.1 ms ($n = 29$; Fig. 2d, e), which may be too short to accommodate two synaptic transmission steps at 32–34 °C (ref. 16). Second, GABAergic conductances preceded or occurred synchronously with EPSCs (Fig. 2d, e), which arise after

glutamate co-release from DA terminals[10–12] (Fig. 2h, i). Third, a population of dopaminergic SNc neurons expresses messenger RNA for glutamic acid decarboxylase (GAD-65)[17], indicating that they may synthesize GABA. We reasoned that if GABA originates from dopaminergic terminals, optically evoked IPSCs, EPSCs and extracellular DA should be similarly affected by pharmacological agents and persist under conditions that prevent disynaptic transmission. Indeed, IPSCs in SPNs were reduced by quinpirole, eliminated by cadmium, but were insensitive to glutamate and DA receptor inhibitors (Fig. 2g), indicating that they require $Ca^{2+}$-dependent release of a transmitter other than glutamate or DA. Moreover, light-evoked IPSCs, EPSCs and DA release were abolished in the presence of the voltage-gated $Na^+$ channel blocker tetrodotoxin (TTX), showing that ChR2-mediated depolarization is not sufficient to trigger transmitter release from nigrostriatal axons (Fig. 2h, i). Neurotransmission can be rescued from directly illuminated ChR2-expressing terminals in the presence of TTX by providing extra depolarization with the voltage-gated $K^+$ channel blocker 4-aminopyridine[18]. Accordingly, IPSCs, EPSCs and DA release recovered upon co-application of TTX and 4-aminopyridine (Fig. 2h, i), indicating that GABA, glutamate and DA are directly released from dopaminergic terminals.

The vesicular GABA transporter VGAT (encoded by *Slc32a1*) is the only transporter known to package GABA into synaptic vesicles and is considered indispensable for inhibitory synaptic transmission[19]. We generated conditional knockout (cKO) mice in which VGAT is specifically deleted from DA neurons (*Slc6a3*$^{IRES-Cre/wt}$;*Slc32a1*$^{lox/lox}$ mice), predicting that ChR2-evoked IPSCs would be abolished. However, light-evoked IPSCs and EPSCs were unaffected in these mice (Fig. 3a, b, g, j), indicating that VGAT is not responsible for vesicular loading of GABA in DA neurons. We instead hypothesized that GAD-65 may synthesize GABA from its metabolic precursor glutamate once inside synaptic vesicles. If correct, preventing glutamate loading into synaptic vesicles by genetically ablating the vesicular glutamate transporter 2 (VGLUT2; encoded by *Slc17a6*) from DA neurons (*Slc6a3*$^{IRES-Cre/wt}$;*Slc17a6*$^{lox/lox}$ mice) should eliminate IPSCs and EPSCs[10]. However, conditional deletion of VGLUT2 abolished light-evoked EPSCs in SPNs without affecting IPSC amplitude or latency (Fig. 3c, g, j), excluding this possibility.

These results indicate that GABA release originates in nigrostriatal terminals but is independent of VGAT and VGLUT2, suggesting the existence of an alternative vesicular transporter with previously unidentified activity for GABA. Consistent with this, IPSCs were eliminated in slices obtained from mice treated with the VMAT2 antagonists reserpine, Ro4-1284 or TBZ and largely recovered upon Ro4-1284 and TBZ washout (Fig. 3d–g). The same manipulation did not affect EPSCs or VGAT-dependent GABA release from SPNs (Supplementary Fig. 5), and we confirmed that DA itself does not function as a $GABA_A$ receptor agonist in SPNs (Supplementary Fig. 6). Moreover, DA depletion with α-methyl-tyrosine (Fig. 1e) had no effect on IPSCs or EPSCs (Fig. 3g). We therefore conclude that VMAT2, but not DA, is required for the release of GABA by DA neurons.

If GABAergic IPSCs depend on VMAT2 solely for GABA transport into synaptic vesicles, IPSCs should be restored in reserpine-treated mice by expressing VGAT in DA neurons (Fig. 3h). Accordingly, in *Slc6a3*$^{IRES-Cre/wt}$ mice injected with AAV encoding Cre-dependent VGAT (AAV-DIO-VGAT) and treated with reserpine, optogenetic stimulation of nigrostriatal axons elicited large SR95531-sensitive IPSCs exhibiting synaptic latencies (Fig. 3g–j) and rise times (1.8 ± 0.3, $n = 10$; $P > 0.05$ versus control, Mann–Whitney rank sum test) indistinguishable from IPSCs observed in untreated mice. Together, these data indicate that presynaptic DA terminals contain GABA, the synaptic packaging of which requires VMAT2 but not VGAT.

VMAT2 transports a variety of substrates[20], including catecholamines, serotonin and histamine. Although GABA does not bear structural resemblance to known VMAT2 substrates, our findings suggest that VMAT2 may function as a vesicular GABA transporter. To test

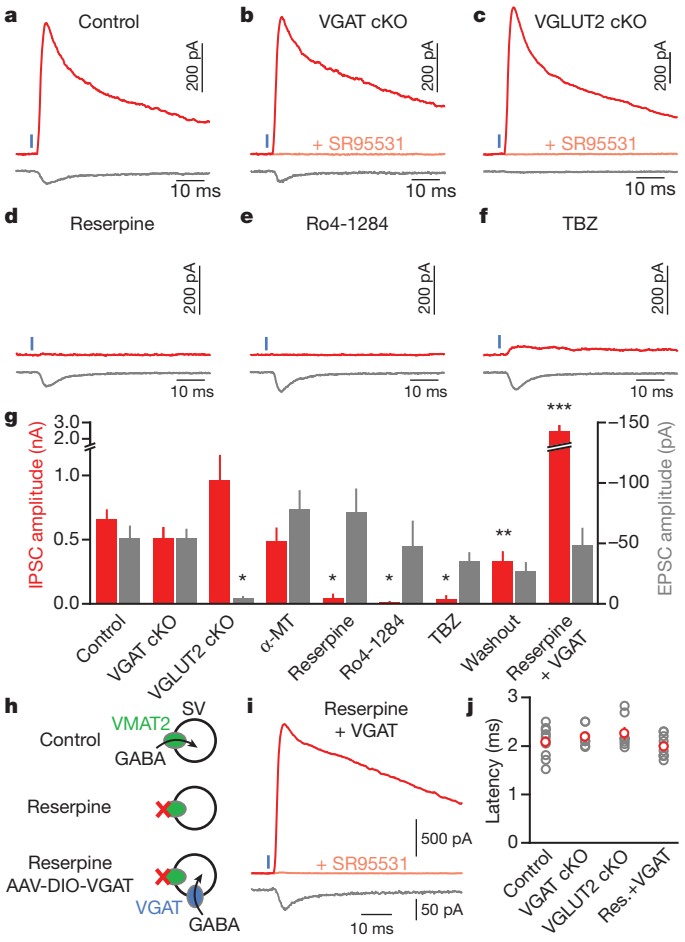


**Figure 3 | GABA release from DA neurons requires VMAT2 but not VGAT.** **a**–**c**, Representative ChR2-evoked (1 ms, blue) IPSCs (red, $V_h = 0$ mV) and EPSCs (grey, $V_h = -70$ mV) from SPNs in *Slc6a3*$^{IRES-Cre/wt}$ (control, **a**), *Slc6a3*$^{IRES-Cre/wt}$;*Slc32a1*$^{lox/lox}$ (VGAT cKO, **b**) and *Slc6a3*$^{IRES-Cre/wt}$;*Slc17a6*$^{lox/lox}$ (VGLUT2 cKO, **c**) mice. **d**–**e**, As in **a** for control *Slc6a3*$^{IRES-Cre/wt}$ mice treated *in vivo* and *in vitro* with the VMAT2 antagonists reserpine (**d**), Ro4-1284 (**e**) or TBZ (**f**). **g**, Mean IPSC (red) and EPSC (grey) amplitudes across conditions ($n = 4$–33). Washout, slices obtained from mice treated *in vivo* with TBZ or Ro4-1284 and subsequently allowed to recover *in vitro* for more than 1 h in ACSF. *$P < 0.05$ versus ACSF; **$P < 0.05$ versus TBZ/Ro4-1284; ***$P < 0.05$ versus reserpine (Kruskal–Wallis analysis of variance). **h**, Schematic of working hypothesis: Provided DA neurons contain cytosolic GABA, viral expression of reserpine-resistant VGAT in DA neurons should rescue GABA transport into synaptic vesicles (SVs) and IPSCs in reserpine-treated mice. Note that VGAT might also incorporate into $VMAT2^-$ vesicles. **i**, Voltage-clamp recording ($V_h = 0$ mV, red; $V_h = -70$ mV, grey) from a reserpine-treated iSPN upon optogenetic stimulation (1 ms, blue) of VGAT-expressing DA axons. **j**, IPSC onset latencies (grey, individual cells; red, average) did not differ across conditions. res., reserpine. GABAergic nature of outward currents ($V_h = 0$ mV) in **b**, **c** and **i** was confirmed with SR95531 (pink). Error bars, s.e.m.

this possibility, we asked if VMAT2 can substitute for VGAT to sustain GABA release in a population of non-monoaminergic GABAergic neurons. Specifically, we attempted to restore GABA release in iSPNs devoid of VGAT by exogenously expressing VMAT2. We conditionally excised the gene encoding VGAT in iSPNs and virally expressed ChR2 in these cells to allow monitoring of GABA release from iSPN axon collaterals onto neighbouring dSPNs as light-evoked IPSCs[21] (Fig. 4a). Whereas optogenetic stimulation of iSPNs in control mice (*Adora2a*-Cre;*Slc32a1*$^{lox/wt}$;*Drd2*-EGFP) reliably evoked large IPSCs in dSPNs, IPSCs were almost entirely abolished in dSPNs from VGAT cKO mice (*Adora2a*-Cre;*Slc32a1*$^{lox/lox}$;*Drd2*-EGFP) (Fig. 4b, c, e), confirming the dependence of vesicular GABA transport in SPNs

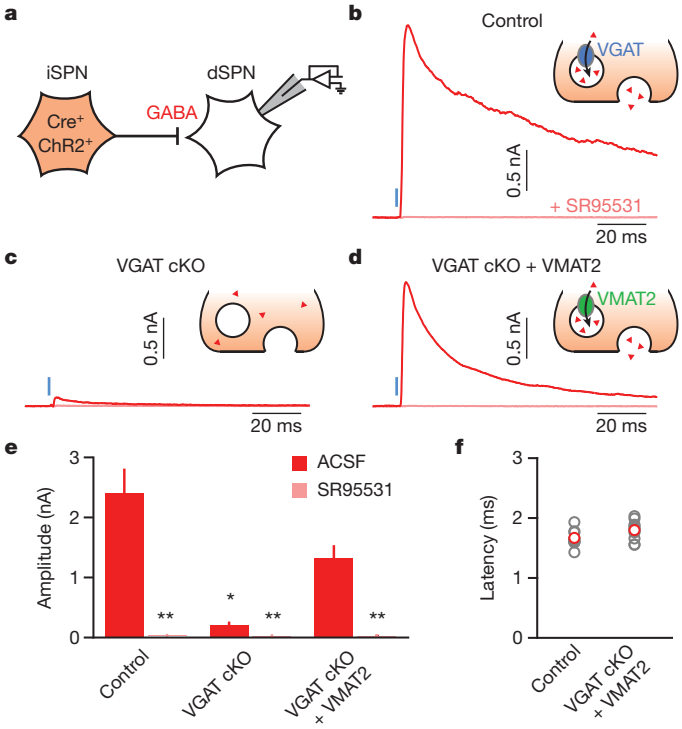


**Figure 4 | VMAT2 functions as a vesicular GABA transporter.** **a**, Experimental setup: ChR2 was selectively expressed in Cre-containing iSPNs of mice with one (control; *Adora2a*-Cre;*Slc32a1*$^{lox/wt}$;*Drd2*-EGFP mice) or both alleles of the gene encoding VGAT flanked by lox sites (VGAT cKO; *Adora2a*-Cre;*Slc32a1*$^{lox/lox}$;*Drd2*-EGFP mice). VGAT cKO + VMAT2, an AAV encoding Cre-dependent VMAT2 (AAV-DIO-VMAT2), was co-injected with AAV-DIO-ChR2 in the striatum of VGAT cKO mice to rescue GABA release from iSPNs. **b**–**d**, Voltage-clamp recordings ($V_h = 0$ mV) of axon-collateral IPSCs in dSPNs evoked by optogenetic stimulation (1 ms, blue) of iSPNs in the absence (red) or presence (pink) of SR95531 in control (**b**), VGAT cKO (**c**) and VGAT cKO + VMAT2 (**d**) mice. Insets: iSPN presynaptic terminal schematic illustrating experimental conditions. Red triangles, GABA. **e**, Summary histogram (mean ± s.e.m.) of experiments in **b**–**d** ($n = 10$–15 dSPNs). *$P < 0.05$ versus control and VGAT cKO+VMAT2 (Kruskal–Wallis analysis of variance); **$P < 0.05$ versus IPSC without SR95531 (Mann–Whitney rank sum test). **f**, IPSC onset latencies from light presentation onset (grey, individual cells; red, mean ± s.e.m.) in control (*Adora2a*-Cre;*Slc32a1*$^{lox/wt}$;*Drd2*-EGFP mice) and VGAT cKO+VMAT2 mice (*Adora2a*-Cre;*Slc32a1*$^{lox/lox}$;*Drd2*-EGFP mice transduced with AAV-DIO-VMAT2 in striatum).

on VGAT[19,21]. By contrast, in VGAT cKO mice transduced with Cre-dependent VMAT2 (AAV-DIO-VMAT2), light reliably evoked large, short-latency IPSCs (Fig. 4d–f). Thus, VMAT2 expression in GABAergic neurons can functionally replace VGAT and sustain inhibitory synaptic transmission.

Midbrain DA neurons are critical for the initiation, selection and reinforcement of motor actions and have been implicated in motor, cognitive and addictive disorders[1–7]. Their effects are largely attributed to the slow neuromodulatory actions of DA receptors[1–3]. Our studies show that DA neurons also exert a rapid and potent inhibitory influence on the activity of SPNs by releasing another transmitter that activates $GABA_A$ receptors. Release of this transmitter depends on VMAT2 activity, indicating that VMAT2 or a molecular complex requiring VMAT2 activity packages it in synaptic vesicles together with DA. The simplest model accounting for our data is that GABA is the transmitter packaged by VMAT2 and released onto SPNs. However, we cannot rule out that another molecule present in iSPNs and DA neurons, acting as a $GABA_A$ receptor agonist, and serving as a substrate for both VMAT2 and VGAT, fulfils that role.

It is estimated that 5–10% of SNc DA neurons express GAD-65 and fewer than 1% express VGLUT2 in rodents[10,17,22]. Therefore, distinct subpopulations of DA neurons may release GABA and glutamate, and reliable detection of IPSCs and EPSCs may result from innervation of SPNs by several DA neurons[23]. Alternatively, GABAergic transmission may be common to midbrain DA neurons as any means of acquiring GABA, such as plasma membrane uptake, would result in vesicular transport. GAD expression varies in response to neuronal activity[24] and damage[25], suggesting that GABAergic signalling from DA neurons may be altered by drug abuse. Our findings also suggest that loss of GABA release in the striatum may contribute to the symptoms of Parkinson's disease as well as to the alterations of striatal circuitry that accompany loss of midbrain DA neurons.

Because all monoaminergic neurons express VMAT2, GABA co-release may extend to adrenergic, noradrenergic, serotonergic, histaminergic as well as other dopaminergic neurons. Indeed, GABA release was reported from dopaminergic amacrine cells in the retina[26] and periglomerular cells in the olfactory bulb[27], although dependence on VMAT2 remains to be determined. Moreover, a considerable fraction (up to 80%) of monoaminergic neurons in locus coeruleus[28], hypothalamus[29] and raphe nuclei[30] contain GABA or express GAD. Together, these findings expand the repertoire of synaptic mechanisms available to monoaminergic cells and suggest that perturbations of GABA co-transmission might contribute to the aetiology of monoaminergic pathologies or to the therapeutic efficacy of VMAT2 antagonists.

## METHODS SUMMARY

Stereotaxic injections of Cre-dependent AAVs were targeted to SNc of postnatal day (P)18–25 *Slc6a3*$^{IRES-Cre/wt}$;*Drd2*-EGFP mice, in which Cre and EGFP are respectively restricted to cells expressing the plasma membrane DA transporter DAT and $D_2$ receptors. Conditional deletion of VGAT or VGLUT2 in these mice was respectively achieved by breeding in *Slc32a1*$^{lox}$ or *Slc17a6*$^{lox}$ alleles to homozygosity. AAVs were allowed to express for at least 21 days before experimentation.

Whole-cell current- and voltage-clamp recordings were obtained from pathway-identified dorsal striatum SPNs in acute parasagittal slices of mature (P40–218) mice at 32–34 °C using standard techniques. Constant-potential amperometry (+400 to 600 mV versus Ag/AgCl) was performed using carbon-fibre microelectrodes. ChR2-expressing fibres were stimulated using brief full-field flashes of blue laser light (1 ms; 473 nm; 6.5–10.0 mW mm$^{-2}$) at intervals of 30 s or more. Traces are the average of three to five consecutive acquisitions. For pharmacological analyses, the peak amplitude of three consecutive light-evoked responses 3–4 min after drug perfusion onset were averaged, normalized to baseline and compared with values obtained at corresponding times in control preparations bathed in artificial cerebrospinal fluid (ACSF). Data in text and figures are reported as mean ± standard error of the mean (s.e.m.). Statistical tests are noted in the text (significance: $P < 0.05$).

**Full Methods** and any associated references are available in the online version of the paper.

**Received 15 May; accepted 27 July 2012.**
**Published online 3 October 2012.**

1. Schultz, W. Predictive reward signal of dopamine neurons. *J. Neurophysiol.* **80,** 1–27 (1998).
2. Wickens, J. R., Reynolds, J. N. & Hyland, B. I. Neural mechanisms of reward-related motor learning. *Curr. Opin. Neurobiol.* **13,** 685–690 (2003).
3. Gerfen, C. R. & Surmeier, D. J. Modulation of striatal projection systems by dopamine. *Annu. Rev. Neurosci.* **34,** 441–466 (2011).
4. Palmiter, R. D. Dopamine signaling in the dorsal striatum is essential for motivated behaviors: lessons from dopamine-deficient mice. *Ann. NY Acad. Sci.* **1129,** 35–46 (2008).
5. Albin, R. L., Young, A. B. & Penney, J. B. The functional anatomy of basal ganglia disorders. *Trends Neurosci.* **12,** 366–375 (1989).
6. Dagher, A. & Robbins, T. W. Personality, addiction, dopamine: insights from Parkinson's disease. *Neuron* **61,** 502–510 (2009).
7. Sulzer, D. How addictive drugs disrupt presynaptic dopamine neurotransmission. *Neuron* **69,** 628–649 (2011).
8. Bentivoglio, M. & Morei, M. in *Handbook of Chemical Neuroanatomy – Dopamine* Vol. 21, 1–107 (Elsevier, 2005).
9. Chuhma, N. *et al.* Dopamine neurons mediate a fast excitatory signal via their glutamatergic synapses. *J. Neurosci.* **24,** 972–981 (2004).
10. Hnasko, T. S. *et al.* Vesicular glutamate transport promotes dopamine storage and glutamate corelease *in vivo*. *Neuron* **65,** 643–656 (2010).
11. Tecuapetla, F. *et al.* Glutamatergic signaling by mesolimbic dopamine neurons in the nucleus accumbens. *J. Neurosci.* **30,** 7105–7110 (2010).

12. Stuber, G. D., Hnasko, T. S., Britt, J. P., Edwards, R. H. & Bonci, A. Dopaminergic terminals in the nucleus accumbens but not the dorsal striatum corelease glutamate. *J. Neurosci.* **30,** 8229–8233 (2010).
13. Boyden, E. S., Zhang, F., Bamberg, E., Nagel, G. & Deisseroth, K. Millisecond-timescale, genetically targeted optical control of neural activity. *Nature Neurosci.* **8,** 1263–1268 (2005).
14. Backman, C. M. *et al.* Characterization of a mouse strain expressing Cre recombinase from the 3′ untranslated region of the dopamine transporter locus. *Genesis* **44,** 383–390 (2006).
15. Schmitz, Y., Benoit-Marand, M., Gonon, F. & Sulzer, D. Presynaptic regulation of dopaminergic neurotransmission. *J. Neurochem.* **87,** 273–289 (2003).
16. Sabatini, B. L. & Regehr, W. G. Timing of synaptic transmission. *Annu. Rev. Physiol.* **61,** 521–542 (1999).
17. Gonzalez-Hernandez, T., Barroso-Chinea, P., Acevedo, A., Salido, E. & Rodriguez, M. Colocalization of tyrosine hydroxylase and GAD65 mRNA in mesostriatal neurons. *Eur. J. Neurosci.* **13,** 57–67 (2001).
18. Cruikshank, S. J., Urabe, H., Nurmikko, A. V. & Connors, B. W. Pathway-specific feedforward circuits between thalamus and neocortex revealed by selective optical stimulation of axons. *Neuron* **65,** 230–245 (2010).
19. Wojcik, S. M. *et al.* A shared vesicular carrier allows synaptic corelease of GABA and glycine. *Neuron* **50,** 575–587 (2006).
20. Yelin, R. & Schuldiner, S. The pharmacological profile of the vesicular monoamine transporter resembles that of multidrug transporters. *FEBS Lett.* **377,** 201–207 (1995).
21. Kozorovitskiy, Y., Saunders, A., Johnson, C. A., Lowell, B. B. & Sabatini, B. L. Recurrent network activity drives striatal synaptogenesis. *Nature* **485,** 646–650 (2012).
22. Berube-Carriere, N. *et al.* The dual dopamine-glutamate phenotype of growing mesencephalic neurons regresses in mature rat brain. *J. Comp. Neurol.* **517,** 873–891 (2009).
23. Matsuda, W. *et al.* Single nigrostriatal dopaminergic neurons form widely spread and highly dense axonal arborizations in the neostriatum. *J. Neurosci.* **29,** 444–453 (2009).
24. Ramirez, M. & Gutierrez, R. Activity-dependent expression of GAD67 in the granule cells of the rat hippocampus. *Brain Res.* **917,** 139–146 (2001).
25. Gonzalez-Hernandez, T., Barroso-Chinea, P. & Rodriguez, M. Response of the GABAergic and dopaminergic mesostriatal projections to the lesion of the contralateral dopaminergic mesostriatal pathway in the rat. *Mov. Disord.* **19,** 1029–1042 (2004).
26. Hirasawa, H., Puopolo, M. & Raviola, E. Extrasynaptic release of GABA by retinal dopaminergic neurons. *J. Neurophysiol.* **102,** 146–158 (2009).
27. Maher, B. J. & Westbrook, G. L. Co-transmission of dopamine and GABA in periglomerular cells. *J. Neurophysiol.* **99,** 1559–1564 (2008).
28. Iijima, K. Chemocytoarchitecture of the rat locus ceruleus. *Histol. Histopathol.* **8,** 581–591 (1993).
29. Trottier, S. *et al.* Co-localization of histamine with GABA but not with galanin in the human tuberomamillary nucleus. *Brain Res.* **939,** 52–64 (2002).
30. Broadbelt, K. G., Paterson, D. S., Rivera, K. D., Trachtenberg, F. L. & Kinney, H. C. Neuroanatomic relationships between the GABAergic and serotonergic systems in the developing human medulla. *Auton. Neurosci.* **154,** 30–41 (2010).

**Supplementary Information** is available in the online version of the paper.

**Acknowledgements** The authors thank A. Saunders and Y. Kozorovitskiy for generating and characterizing the AAV-DIO-EGFP and AAV-DIO-VGAT constructs, D. Sulzer and H. Zhang for assistance with amperometry, R. Shah and C. Johnson for technical support, and members of the laboratory for discussions. This work was supported by a Nancy Lurie Marks Family Foundation postdoctoral fellowship (N.X.T.) and by grants from the National Institutes of Health (NS046579 to B.L.S. and 4R00NS075136 to J.B.D.).

**Author Contributions** N.X.T., J.B.D. and B.L.S. designed the experiments. N.X.T. performed the experiments described in the figures and text and analysed the data. J.B.D. performed experiments that initiated this study, devised the injection coordinates, established amperometric recordings and participated in their acquisition. N.X.T. and B.L.S. wrote the manuscript with contributions from J.B.D.

**Author Information** Reprints and permissions information is available at www.nature.com/reprints. The authors declare no competing financial interests. Readers are welcome to comment on the online version of the paper. Correspondence and requests for materials should be addressed to B.L.S. (bsabatini@hms.harvard.edu).

## METHODS

**Mice.** Knock-in mice bearing an internal ribosome entry site (IRES)-linked Cre recombinase gene downstream of the gene *Slc6a3*, which encodes the plasma membrane DA transporter DAT (referred to as *Slc6a3*$^{IRES-Cre}$ mice)[14] were obtained from the Jackson Laboratory (stock number 006660). Homozygous (*Slc6a3*$^{IRES-Cre/IRES-Cre}$) and heterozygous (*Slc6a3*$^{IRES-Cre/wt}$) animals were bred with *Drd2*-EGFP transgenic mice (GENSAT, founder line S118), which express EGFP under control of a bacterial artificial chromosome containing the $D_2$ receptor genomic locus to permit distinction between direct- and indirect-pathway SPNs[31]. Alternatively, *Slc6a3*$^{IRES-Cre}$ mice were crossed with mice bearing a Cre-dependent TdTomato reporter transgene (Ai14; the Jackson Laboratory, stock number 007914; referred to as *Rosa26*$^{lsl-tdtomato}$ mice) to show the distribution of Cre$^+$ cells[32]. Mice in which the second exon of *Slc32a1*, which encodes the vesicular GABA transporter (VGAT), or *Slc17a6*, which encodes the vesicular glutamate transporter 2 (VGLUT2), is flanked by lox sites (*Slc32a1*$^{lox}$ and *Slc17a6*$^{lox}$, respectively) were provided by B. Lowell[33,34]. Conditional deletion of VGAT or VGLUT2 from Cre-expressing DA neurons was achieved by crossing *Slc6a3*$^{IRES-Cre/wt}$;*Slc32a1*$^{lox/wt}$ and *Slc32a1*$^{lox/lox}$;*Drd2*-EGFP mice, or *Slc6a3*$^{IRES-Cre/wt}$;*Slc17a6*$^{lox/wt}$ and *Slc17a6*$^{lox/lox}$ mice, respectively. No differences were observed between control *Slc6a3*$^{IRES-Cre}$ mice and *Slc6a3*$^{IRES-Cre}$ mice carrying a single floxed allele of *Slc32a1* or *Slc17a6*, so data from these animals were pooled. iSPNs were genetically targeted using *Adora2a*-Cre bacterial artificial chromosome transgenic mice (GENSAT, founder line KG139), which express Cre under transcriptional control of the adenosine $A_{2A}$ receptor genomic promoter[35]. Conditional deletion of VGAT in Cre-expressing iSPNs was achieved by crossing *Adora2a*-Cre;*Slc32a1*$^{lox/wt}$ and *Slc32a1*$^{lox/lox}$;*Drd2*-EGFP mice. Other lines used included *Th*-Cre transgenic mice (the Jackson Laboratory, stock number 008601) and *Drd1a*-Cre bacterial artificial chromosome transgenic mice (GENSAT, founder line EY262). With the exception of *Slc6a3*$^{IRES-Cre}$ and *Rosa26*$^{lsl-tdtomato}$ mice, which were maintained on a C57BL/6 background, all other strains were maintained on a mixed background of C57BL/6 and FVB. All experimental manipulations were performed in accordance with protocols approved by the Harvard Standing Committee on Animal Care following guidelines described in the US National Institutes of Health *Guide for the Care and Use of Laboratory Animals*.

**Virus preparation.** Conditional expression of the light-gated non-selective cation channel channelrhodopsin-2 (ChR2, H134R variant) in Cre-containing neurons was achieved using a recombinant AAV encoding a double-floxed inverted open reading frame (DIO) of the ChR2–mCherry fusion protein under transcriptional control of the EF1α promoter (AAV-DIO–ChR2; http://www.stanford.edu/group/dlab/optogenetics/sequence_info.html#dio). Cre-dependent AAV vectors encoding EGFP (AAV-DIO-EGFP), VGAT (NM_009508.2; AAV-DIO-VGAT; Addgene plasmid 39320) or VMAT2 (NM_172523.3; AAV-DIO-VMAT2; Addgene plasmid 39339) were generated by replacing the ChR2–mCherry coding sequence using Asc1 and Nhe1 restriction sites (Genscript). These viral vectors were subsequently packaged (serotype 8) by a commercial vector core facility (University of North Carolina). All AAVs were stored in undiluted aliquots at a working concentration of at least $10^{12}$ genomic copies per millilitre at −80 °C until intracranial injection.

**Stereotaxic intracranial injections.** Male and female mice (P18–25) were anaesthetized with isoflurane and placed in a small animal stereotaxic frame (David Kopf Instruments). After exposing the skull under aseptic conditions, a small burr hole was drilled and AAVs were injected (0.5–1 μl total volume) unilaterally through a pulled glass pipette at a rate of 100 nl min$^{-1}$ using a UMP3 microsyringe pump (World Precision Instruments). Injection coordinates were 0.8 mm anterior from Lambda, 1.3 mm lateral and 4.4 mm below pia for SNc, and 0.5 mm anterior from Bregma, 1.75 mm lateral, and 2.7 mm below pia for dorsal striatum. After surgical procedures, mice were returned to their home cage at least 21 days to allow for maximal gene expression. To identify striatum-projecting neurons in ventral midbrain, *Slc6a3*$^{IRES-Cre/wt}$;*Rosa26*$^{lsl-tdtomato/wt}$ mice were injected with 0.1–0.2 μl fluorescent latex microspheres (Green Retrobeads, Lumafluor) in dorsal striatum (same coordinates as above) and allowed to recover in their home cage for 7 days before processing their brain for tyrosine hydroxylase immunolabelling.

**Immunocytochemistry.** Mice were deeply anaesthetized with isoflurane and perfused transcardially with 4% paraformaldehyde in 0.1 M sodium phosphate buffer. Brains were post-fixed for 1–3 days, washed in phosphate buffered saline (PBS) and sectioned (40–50 μm) coronally (Vibratome). Free-floating sections were permeabilized/blocked with 5% normal goat serum in PBS with 0.3% Triton X-100 (PBST) for 2 h at room temperature and incubated with primary antibodies at 4 °C overnight and with secondary antibodies for 2 h at room temperature in PBST supplemented with 1% normal goat serum. Brain sections were mounted on superfrost slides, dried and coverslipped with ProLong antifade reagent with DAPI (Molecular Probes). Primary antibodies used included rabbit anti-tyrosine-hydroxylase (1:2,000; AB152, Millipore), mouse anti-tyrosine-hydroxylase (1:1,000; 22941, ImmunoStar) and rabbit anti-VMAT2 (1:2,000; ab81855, Abcam). Alexa Fluor 488- and 647-conjugated secondary antibodies to rabbit and mouse (Invitrogen) were diluted 1:1,000. Endogenous TdTomato and EGFP fluorescences were not immuno-enhanced. Whole sections were imaged with an Olympus VS110 slide scanning microscope. High-resolution images of regions of interest were subsequently acquired with a Zeiss LSM 510 META confocal microscope (Harvard NeuroDiscovery Center). Images represent maximum intensity projections of 3–7 μm confocal stacks.

**Slice preparation.** Acute brain slices were obtained from 40- to 218-day-old mice (median = 74 days) using standard techniques. Mice were anaesthetized by isoflurane inhalation and perfused cardiacly with ice-cold ACSF containing (in mM) 125 NaCl, 2.5 KCl, 25 $NaHCO_3$, 2 $CaCl_2$, 1 $MgCl_2$, 1.25 $NaH_2PO_4$ and 11 glucose (295 mOsm kg$^{-1}$). Cerebral hemispheres were removed, placed in cold choline-based cutting solution (consisting of (in mM): 110 choline chloride, 25 $NaHCO_3$, 2.5 KCl, 7 $MgCl_2$, 0.5 $CaCl_2$, 1.25 $NaH_2PO_4$, 25 glucose, 11.6 ascorbic acid, and 3.1 pyruvic acid), blocked and transferred into a slicing chamber containing ice-cold choline-based cutting solution. Parasagittal slices of striatum (275 μm thick) were cut with a Leica VT1000 s vibratome, transferred for 10–20 min to a holding chamber containing ACSF at 34 °C and subsequently maintained at room temperature (20–22 °C) until use. All recordings were obtained within 4 h of slicing. Both cutting solution and ACSF were constantly bubbled with 95% $O_2$/5% $CO_2$.

**Electrophysiology.** Individual slices were transferred to a recording chamber mounted on an upright microscope (Olympus BX51WI) and continuously superfused (2–3 ml min$^{-1}$) with ACSF warmed to 32–34 °C by passing it through a feedback-controlled in-line heater (SH-27B; Warner Instruments). Cells were visualized through a ×40 water-immersion objective with either infrared differential interference contrast optics or epifluorescence to identify EGFP$^+$ iSPNs and striatal regions showing the highest density of ChR2–mCherry$^+$ axonal arbors. Epifluorescence was used sparingly to minimize ChR2 activation before recording. Whole-cell voltage- and current-clamp recordings were made from dSPNs or iSPNs in anterior dorsolateral and dorsomedial striatum within 300 μm of the callosal-striatal border. dSPNs and iSPNs were identified on the basis of the respective absence or presence of EGFP fluorescence and their firing properties. Patch pipettes (2–4 MΩ) pulled from borosilicate glass (G150F-3, Warner Instruments) were filled either with a $Cs^+$-based low $Cl^-$ internal solution containing (in mM) 135 $CsMeSO_3$, 10 HEPES, 1 EGTA, 3.3 QX-314 ($Cl^-$ salt), 4 Mg-ATP, 0.3 Na-GTP, 8 $Na_2$-phosphocreatine (pH 7.3 adjusted with CsOH; 295 mOsm·kg$^{-1}$) for voltage-clamp recordings, or with a $K^+$-based low $Cl^-$ internal solution composed of (in mM) 135 $KMeSO_3$, 3 KCl, 10 HEPES, 1 EGTA, 0.1 $CaCl_2$, 4 Mg-ATP, 0.3 Na-GTP, 8 $Na_2$-phosphocreatine (pH 7.3 adjusted with KOH; 295 mOsm·kg$^{-1}$) for current-clamp recordings. Bath solutions for whole-cell recordings did not contain drugs unless specified otherwise. For all voltage-clamp experiments, errors due to the voltage drop across the series resistance (<20 MΩ) were left uncompensated. Membrane potentials were corrected for a ~8 mV liquid junction potential. To activate ChR2-expressing fibres, light from a 473 nm laser (Optoengine) was focused on the back aperture of the microscope objective to produce wide-field illumination of the recorded cell. Brief pulses of light (1 ms duration; 6.5–10.0 mW mm$^{-2}$ under the objective) were delivered at the recording site at 30 s intervals under control of the acquisition software. For current-clamp recordings, depolarizing current steps evoking 10–20 Hz trains of action potentials were applied at regular intervals (10–15 s) either alone or in combination with a 1 ms flash of blue light.

**Amperometric recordings.** Constant-potential amperometry was performed using homemade glass-encased carbon-fibre microelectrodes (7 μm diameter, 50–100 μm length) placed approximately 50 μm within dorsal striatum slices and held at a constant voltage of +400 to 600 mV versus Ag/AgCl by a Multiclamp 700B amplifier (Molecular Devices). Electrodes were calibrated with fresh 5 μM dopamine standards in ACSF using fast-scanning cyclic voltammetry (from −0.5 V to 0.9 V, and back to −0.5 V at a rate of 280 mV ms$^{-1}$ every 100 ms, with the electrode held at 0 V between scans) to determine the optimal oxidation potential, followed by constant-potential amperometry of dopamine flow-in to allow conversion of current amplitude to extracellular dopamine concentration. Dopaminergic terminals surrounding the electrode were stimulated with 1 ms flashes of blue laser light (6.5–10.0 mW mm$^{-2}$) delivered at 2–3 min intervals.

**Reagents.** Drugs (all from Tocris, unless specified otherwise) were applied by bath perfusion: SR95531 (10 μM), (-)biccuculine (20 μM), (1,2,5,6-tetrahydropyridin-4-yl)methylphosphinic acid (TPMPA; 20 μM), 2,3-dihydroxy-6-nitro-7-sulfamoyl-benzo(*f*)quinoxaline (NBQX; 10 μM), *R*,*S*-3-(2-carboxypiperazin-4-yl)propyl-1-phosphonic acid (CPP; 10 μM), tetrodotoxin (TTX; 1 μM), 4-aminopyridine (4AP; 0.1–1 mM), $CdCl_2$ (Sigma, 30 μM) and (−)quinpirole (10 μM). The cocktail of antagonists used broadly to target $D_1$ and $D_2$ receptor families ($D_{1/2}$R

antagonists) consisted of SCH23390 (1 μM), SKF83566 (1 μM), (−)sulpiride (10 μM) and L-741,626 (1 μM). To inhibit monoaminergic vesicular transport and deplete transmitter-filled vesicles, *Slc6a3*$^{IRES-Cre}$ mice were injected intraperitoneally with either the irreversible VMAT inhibitor reserpine (5 mg kg$^{-1}$) 24 h before slicing, the reversible VMAT antagonist Ro4-1284 (Sigma, 15 mg kg$^{-1}$) 1 h before slicing or the competitive and selective VMAT2 antagonist tetrabenazine (TBZ; 5 mg kg$^{-1}$) 2 h before slicing. To deplete presynaptic terminals of dopamine, *Slc6a3*$^{IRES-Cre}$ mice were administered the tyrosine hydroxylase antagonist α-methyl-DL-tyrosine methyl ester hydrochloride (Sigma, 250 mg kg$^{-1}$ intraperitoneally) 3 h and 1 h before slicing. Brain sections from these animals were prepared as described above, but were recovered and incubated in ACSF containing 1 μM reserpine, 10 μM Ro4-1284, 50 μM TBZ or 30 μM α-methyl-tyrosine, respectively. Half of the slices obtained from Ro4-1284- and TBZ-treated mice were kept at least 1 h in regular ACSF before recording to allow for drug washout and resumption of neurotransmitter transport into synaptic vesicles (washout condition in Figs 1e and 3g).

**Data acquisition and analysis.** Membrane currents and potentials were amplified and low-pass filtered at 3 kHz using a Multiclamp 700B amplifier (Molecular Devices), digitized at 10 kHz and acquired using National Instruments acquisition boards and a custom version of ScanImage written in MATLAB (Mathworks)[36]. Amperometry, electrophysiology and imaging data were analysed offline using Igor Pro (Wavemetrics) and ImageJ (National Institutes of Health). In figures, amperometry and voltage-clamp traces represent the averaged waveform of three to five consecutive acquisitions. Detection threshold for IPSCs and EPSCs was set at 10 pA. Averaged waveforms were used to obtain current latency, peak amplitude, 10–90% rise time and decay time. Current onset was measured using a threshold set at three standard deviations of baseline noise. Peak amplitudes were calculated by averaging over a 2 ms window around the peak. For pharmacological analyses in Figs 1e and 2f, g, i, the peak amplitudes of three consecutive light-evoked responses 3–4 min after drug perfusion onset were averaged, normalized to baseline averages and compared statistically with values obtained at corresponding times in control preparations bathed in ACSF. Data (reported in text and figures as mean ± s.e.m.) were compared statistically using the following: Mann–Whitney rank sum test, Kruskal–Wallis analysis of variance (ANOVA) with Dunn's multiple comparison test, and two-way ANOVA followed by Bonferroni post-hoc tests, as indicated in the text. *P* values less than 0.05 were considered statistically significant.


31. Gong, S. *et al.* A gene expression atlas of the central nervous system based on bacterial artificial chromosomes. *Nature* **425,** 917–925 (2003).
32. Madisen, L. *et al.* A robust and high-throughput Cre reporting and characterization system for the whole mouse brain. *Nature Neurosci.* **13,** 133–140 (2010).
33. Tong, Q. *et al.* Synaptic glutamate release by ventromedial hypothalamic neurons is part of the neurocircuitry that prevents hypoglycemia. *Cell Metab.* **5,** 383–393 (2007).
34. Tong, Q., Ye, C. P., Jones, J. E., Elmquist, J. K. & Lowell, B. B. Synaptic release of GABA by AgRP neurons is required for normal regulation of energy balance. *Nature Neurosci.* **11,** 998–1000 (2008).
35. Durieux, P. F. *et al.* D2R striatopallidal neurons inhibit both locomotor and drug reward processes. *Nature Neurosci.* **12,** 393–395 (2009).
36. Pologruto, T. A., Sabatini, B. L. & Svoboda, K. ScanImage: flexible software for operating laser scanning microscopes. *Biomed. Eng. Online* **2,** 13 (2003).